Available online at www.sciencedirect.com
SCIENCE DIRECT®
Journal of Catalysis 222 (2004) 6–16
JOURNAL OF CATALYSIS
www.elsevier.com/locate/jcat

Mechanistic studies of initial decay of hydrodemetallization catalysts using model compounds—effects of adsorption of metal species on alumina support

Fei Xiang Long, Börje S. Gevert,* and Peter Abrahamsson [1]

Department of Materials and Surface Chemistry, Chalmers University of Technology, 412 96 Göteborg, Sweden

Received 2 April 2003; revised 18 August 2003; accepted 24 October 2003

Abstract

Mechanistic studies of the initial decay of hydrodemetallization (HDM) catalysts are performed in a fixed-bed reactor using metalloporphyrins as model compounds. Adsorption of the metalloporphyrins on alumina is quantitatively confirmed, and the metal deposition is proven to have some autocatalytic activity especially hydrogenation activity instead of being a poison. The autocatalytic activity is increased with the metal accumulation on alumina to some extent. However, these metal deposits are still far inferior to commercial HDM catalysts for removing the metals from the stream. Instead of interpreting the initially declining activity as a result of catalyst deactivation, a simultaneous adsorption and reaction mechanism is first proposed in this study. The initial apparent activity is an effect of a nearly constant catalytic activity of the active phase coupled with an extra decreasing adsorption on the alumina support. Consequently, the model based on the new mechanism fits the experimental data reasonably well.

Keywords: Metalloporphyrin; Metal etioporphyrin; Hydroprocessing; Hydrotreating; Hydrodemetallization; HDM; Catalyst deactivation mechanism; Initial stability of HDM catalysts; Adsorption on alumina; Poisoning of metal deposits

1. Introduction

As the first stage of heavy fraction upgrading by hydroprocessing, hydrodemetallization (HDM) is of commercial importance in oil refineries. However, in practice HDM catalysts suffer from a loss of apparent activity, which exhibits an S-shape temperature versus time-on-stream curve when the process is operated at a constant conversion. The decaying curve can be typically subdivided into three distinct sections: an initial rapidly declining period, an intermediate gradually aging period, and an ultimate fast decreasing period [1–6]. In the literature, this phenomenon is attributed to "catalyst deactivation," which is commonly assigned to the accumulation of carbonaceous and metallic deposits on the catalysts [1–31].

Catalyst deactivation can occur basically by mechanisms such as fouling, poisoning, sintering, and evaporating of the active phase [32]. Generally it is acknowledged that carbonaceous deposits or fouling by coke may play a role in the initial stage, depending on the composition of feeds, the characteristics of catalysts, and the severity of reactions [1,2, 7–22]. Noticeably about 10–30 wt% carbonaceous deposits based on the fresh catalyst accumulate on the surface within at most the first 2 weeks of operation, and then attains a quasi-steady state [1,11,12,15,16,18–20]. As a result, nearly 50–60% of the surface area and one-third of the porosity of the original catalyst are lost, which is thought to have an impact on the apparent activity [1,11,12,16,18,20].

Nevertheless, coke formatting and its eventual equilibrium have been argued to be much shorter than the initial decay period lasting 1 to 2 months or a quarter of the effective lifetime of the catalysts [4,10,17,30]. The latest studies find that coke preferentially deposits on the alumina support rather than on the active phase [15,19,31,33,34], suggesting that coking does not foul the active sites substantially. Since a stationary coke level is readily established under a suf-

* Corresponding author.
E-mail address: gevert@surfchem.chalmers.se (B.S. Gevert).
[1] Present address: Preem Oil Refinery, Box 48084, 418 23 Göteborg, Sweden.

0021-9517/$ – see front matter
doi:10.1016/j.jcat.2003.10.025

ficiently high hydrogen pressure, few deactivation models consider coking in predicting the stability of HDM catalysts [4,5]. Therefore, carbonaceous deposition is usually not considered as a serious problem in most industrial operations.

On the other hand, a number of researchers focus on the effects of metallic deposits, mainly vanadium and nickel sulfides, on the initial decay of the catalysts [4–6,26–31]. It has been confirmed that the apparent activity decreases with the increase of the metallic deposition on the surface. Moreover, the length of the initial period is related to the organometallic concentration in the feed [4], which is long enough to form a monolayer coverage usually in the range of 0.034–0.176 g of metals/cm^3 of catalyst [4,18]. Thereby, most modeling works use the deposited metals as an index of catalyst aging, neglecting the contribution of the quick coking. Since only a small quantity of metal deposits builds up on the catalysts in the initial stage, a poisoning mechanism is mostly proposed [26–31].

However, it has been reported that the activity of HDM catalysts does not change significantly after loaded 2–100 wt% metals during the catalytic demetallization of model compounds [35–37]. On the contrary, bare alumina supports or very low initial activity catalysts obtain a certain catalytic activity with the buildup of metal sulfides on the surface in hydroprocessing real petroleum feedstocks or model compounds [38–41]. Furthermore, if the poisoning "deactivation" mechanism is adopted as the mechanism of the initial decay, many questions concerning the effects of the poisons in the whole catalyst life will be raised. It must be explained how the metal deposition deactivates the active phase so efficiently within a short time in a little amount, and then becomes almost nonpoisonous at the long steady deactivation stage in a large quantity. If autocatalytic effects of the metal deposits are assumed, it must be shown how vanadium or nickel sulfides become so active as to decompose the metal species so much over a long time. In that case, to our best knowledge, it is strange that commercial hydroprocessing catalysts use CoMo, NiMo, or NiW as the active elements instead of V or Ni [23,24].

As a matter of fact, many mechanisms could explain the metal deposition on the surface in the initial period, without necessarily demanding that these solids be catalytic. Also the initially decreasing activity does not have to be interpreted as catalyst deactivation. In their batch tests with 2 h of contact time, Gualda and Kasztelan found that the demetallization conversions by alumina alone could reach 75–84% of a $NiMo/Al_2O_3$ catalyst [31]. Therefore, the initial decay of the apparent activity may also be an effect of a nearly constant catalytic activity of the active phase in combination with a decreasing adsorption on the alumina support when the available sites are gradually and continuously occupied. The objective of this fundamental study is to ascertain the role of alumina carriers in the initial decay of HDM catalysts.

2. Experimental

Due to the complex multicomponent systems of oil streams, the depositing patterns of coke and metals can vary with the composition of feedstocks to a large extent. It is very difficult to distinguish quantitatively the contribution of each factor to the decay of HDM catalysts during hydroprocessing real petroleum feeds. In order to avoid ambiguous results caused by the possible influence of carbonaceous deposits, model compounds were chosen to elucidate the role of metal deposition in the initial decay.

In crude oils, vanadium and nickel are the most abundant metals and exist in porphyrinic and nonporphyrinic organometallic complexes [23]. Metals in porphyrinic forms can account for 5–70% of the total metal content in petroleum [42], and 6–34 wt% of vanadium and nickel compounds falls into metalloporphyrins [23]. Since etio-type metalloporphyrins naturally occur in petroleum and constitute up to 50% of the metals in the free porphyrin fraction [43], vanadyl etioporphyrin (VO-EP) and nickel etioporphyrin (Ni-EP) whose molecular structures are shown in Fig. 1 were selected as the model compounds in this study. Feeds for the model compound studies were prepared by dissolving VO-EP or Ni-EP (Midcentury Chemicals, Posen, IL) into white oil (Nypol 68, Nynäs Petroleum, Sweden) at 523 K under the protection of nitrogen for 3 h of agitation. The maximum concentration obtained of vanadium or nickel in the solution was around 40 ppm. In several runs, in order to investigate the effects of competitive adsorption on surface, 2,6-dimethylpyridine or 3,5-dimethylpyridine was introduced into the stream.

Three kinds of materials were utilized in this work to study adsorption and/or reactions of the metalloporphyrins on the surface. Solid glass beads of sodium glass (Kebo, Sweden) were representative of the materials that were inert in the catalytic reactions and had little surface area for adsorption. Alumina extrudates produced from hydration of trialkylaluminum at Condea in Germany were typical porous supports for hydroprocessing catalysts and were used as received. Commercial $CoMo/Al_2O_3$ HDM catalyst TK-710 (Haldor Topsoe AS, Lyngby, Denmark) in the shape of 1/32-in. extrudates was sulfided in situ before the experiments began. The sulfidation was achieved with a mixture

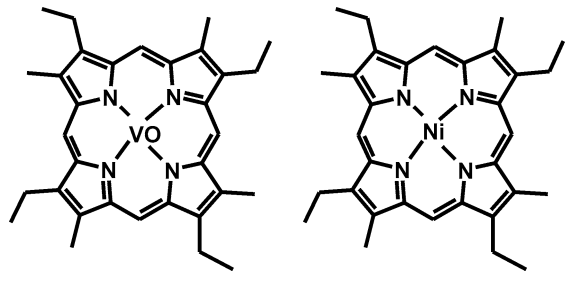

(a) (b)

Fig. 1. Molecular structures of metalloporphyrins: (a) vanadyl etioporphyrin (VO-EP); (b) nickel etioporphyrin (Ni-EP).

Table 1
Chemical and physical properties of materials used in the experiments

		Material		
		Glass beads	Alumina	TK-710
Shape		Spherical	Cylindrical	Cylindrical
Diameter (mm)		4	3	0.8
Composition (wt%)	MoO_3	0	0	6[a]
	CoO	0	0	2[a]
Surface area (m^2/g)		6×10^{-4}	213	140[b]
Pore volume (cm^3/g)		0.00	0.63	0.57[b]
Particle density (g/cm^3)		–	1.38	1.08
Bed density (g/cm^3)		1.35	0.62	0.64

[a] From Ref. [44].
[b] From Ref. [45].

of 10 vol% of hydrogen sulfide in hydrogen at a pressure of 0.4 MPa, a flow rate of 100 N ml/h, and a temperature of 673 K for 4 h. During runs with the sulfided catalysts, 0.5% of S in CS_2 was added into the feed to maintain the sulfidation level. The basic chemical and physical properties of the three materials are listed in Table 1.

Experiments were performed in a down-flow trickle-bed reactor with an internal diameter of 18 mm and two independent heating zones [45]. Catalysts or alumina extrudates were loaded in the middle of the reactor and the void space above and below was filled with glass beads. Oils fed by a reciprocal pump were mixed with hydrogen or nitrogen before entering the reactor, and samples were withdrawn periodically from the separator. A typical experiment started on heating the reactor at a rate of 10 K per minute under a flow of hydrogen or nitrogen. When the desired temperature was reached, the pressure was raised to the set point, and the oil was pumped while the time was recorded as zero.

It is widely accepted that metalloporphyrins are decomposed under hydrogen via a sequential mechanism involving at least one hydrogenation step and one hydrogenolysis step [36,42,46–50]. To determine the concentrations of the porphyrinic reactants as well as the reaction intermediates, an ultraviolet-visible spectrophotometer (UV-160A, Shimadzu, Japan) was routinely employed to analyze the liquid samples after dilution with white oil. Calibration factors for the porphyrinic species were 0.56 Abs/ppm V for VO-EP (571.5 nm), 0.61 Abs/ppm V for vanadyl etiochlorin (VO-EPH_2, 631 nm), 0.478 Abs/ppm Ni for Ni-EP (552 nm), and 0.72 Abs/ppm Ni for nickel etiochlorin (Ni-EPH_2, 616 nm) [46,47]. To confirm the metal concentration determined by the UV spectrophotometer, some of the samples were also ashed by sulfuric acid according to ASTM D 1548-83. Then the ash was dissolved into a mixture of sulfuric and nitric acid, and after dilution the concentration of vanadium or nickel was analyzed using atomic absorption spectrophotometry (AAS). All of the experimental runs are given in Table 2.

3. Mathematical methods

Mathematical methods combining mass-transfer effects with the proposed disappearance mechanisms of the metal species were developed to predict the performance of the fixed-bed reactor and to interpret the experimental observations. For the disappearance of the metal species, several different mechanisms were suggested and investigated. First, the species having diffused into the porous particle were consumed only by adsorption on alumina supports or on HDM catalysts when inert gas was introduced to prevent the chemical reactions. In this case, a nonlinear Langmuir adsorption

Table 2
Summary of experimental runs

Run	Experimental conditions						
	Material	Volume (cm^3)	Temperature (K)	P (MPa)	v_0 (cm^3/h)	CEP_0 (ppm)	$CEPH_0$ (ppm)
VP-1	Glass beads		523–693	7	16	25.107	1.967
VP-2	Glass beads		613–693	1–7	16	43.250	0.328
VP-3	Alumina	11	523	7	16	42.893	0.361
VP-4	Alumina	22	523	7	16	42.893	0.361
VP-5	Alumina	11	593	7	16	42.893	0.361
VP-6	Alumina	22	613	7	16	23.643	
VP-7	TK-710	3	573	5	16	18.536	1.869
VP-8	TK-710	5	553–593	2–8	17.5–24.8	44.214	0.426
NiP-1	Glass beads		553–673	7	16	37.782	0.625
NiP-2	Glass beads		508–658	7	16	34.289	0.444
NiP-3	Alumina	22	523	7	16	40.203	≈ 0
NiP-4	Alumina	11	593	7	16	43.757	≈ 0
NiP-5	Alumina	22	613	7	16	26.485	
NiP-6	TK-710	5	523	7 (N_2)	16	40.586	≈ 0
NiP-7	TK-710	5	503–523	5	41–46	40.586	≈ 0
NiP-8	TK-710	3	573	5	16	17.824	1.875

P, total pressure; v_0, volumetric flow rate; CEP_0, metal concentration of the etio-type metalloporphyrins in the feed; $CEPH_0$, metal concentration of the dihydrogenated species in the feed.

isotherm was thought favorable. Secondly, the species disappearance was totally attributed to demetallization reactions of the catalysts in a steady state, while a power-law rate expression was chosen. Thirdly, simultaneous adsorption and reaction occurring on different sites of the catalyst surface were considered. Two steps usually involved in modeling the performance of the fixed-bed reactor are based on the different mechanisms: establishing the differential equation of the mass balance for the fluid concentration within the particle and building the differential equation of the material balance for the reactor.

For an isothermal cylindrical particle when film mass-transfer resistance is negligible and pore diffusion is dominated, the differential pseudo-steady-state mass balance for the fluid concentration within the particle C_i yields

$$D_\mathrm{e}\left(\frac{\partial^2 C_\mathrm{i}}{\partial r^2}+\frac{1}{r}\frac{\partial C_\mathrm{i}}{\partial r}\right)+N_\mathrm{i}(t,C_\mathrm{i},T)=0 \tag{1}$$

with initial and boundary conditions

$$C_\mathrm{i}=C_\mathrm{b};\quad t\geqslant 0;\quad r=R_0, \tag{2}$$

$$\frac{\partial C_\mathrm{i}}{\partial r}=0;\quad t\geqslant 0;\quad r=0, \tag{3}$$

where D_e represents the effective diffusivity, r is the radial coordinate of the particle, and R_0 is the radius, N_i denotes the disappearance rate of the species per unit volume of the particle as a function of process time t, concentration C_i, and temperature T, and C_b is the bulk stream concentration of the species.

As for the adsorption mechanism, N_i is expressed as

$$-N_\mathrm{i}=\rho_\mathrm{c}\frac{\partial q}{\partial t}=\rho_\mathrm{c}S_\mathrm{a}\frac{\partial q^*}{\partial t}=\rho_\mathrm{c}S_\mathrm{a}\frac{Kq_0^*}{(1+KC_\mathrm{i})^2}\frac{\partial C_\mathrm{i}}{\partial t}, \tag{4}$$

where ρ_c is the density of the particle, q and q^* denote the quantity of the species adsorbed on the surface per unit weight and per unit surface area, respectively, q_0^* represents the maximum quantity of the species adsorbed on the surface per unit surface area, S_a is the surface area per unit mass of the particle, and K is the adsorption equilibrium constant for the Langmuir isotherm. In the case of the simultaneous adsorption and reaction mechanism, N_i is given by

$$-N_\mathrm{i}=\rho_\mathrm{c}S_\mathrm{a}\frac{Kq_0^*}{(1+KC_\mathrm{i})^2}\frac{\partial C_\mathrm{i}}{\partial t}+k_\mathrm{i}S_\mathrm{a}\rho_\mathrm{c}P^mC_\mathrm{i}^n, \tag{5}$$

where k_i denotes the rate constant of the intrinsic reaction, P is the total pressure, m represents the reaction order with respect to the total pressure, and n is the surface reaction order. Equation (1) is a two-point boundary value problem, which was solved numerically in this study by using the finite element method (FEM) on commercial software MATLAB 5.3. The results are expressed in the form of concentration profiles $C_\mathrm{i}(t,r)$ and concentration gradients $(\partial C_\mathrm{i}/\partial r)(t,r)$ inside the particle at different times on stream.

With the results of a single particle, we now consider the situation that the disappearance of the species takes place in a plug-flow fixed bed with no concentration gradients along the bed under a steady and isothermal state. If the axial dispersion is negligible, the differential equation of the material balance for the bed is given by

$$-\frac{v_0}{A_\mathrm{c}}\frac{dC_\mathrm{b}}{dz}=\frac{2(1-\varepsilon)D_\mathrm{e}}{R_0}\frac{\partial C_\mathrm{i}}{\partial r}\bigg|r=R_0, \tag{6}$$

where v_0 denotes the volumetric flow rate, A_c and z are the cross-sectional area and the axial position of the bed, respectively, and ε represents the bed void fraction. If C_0 denotes the feed concentration of the species, with the aid of the boundary condition at the entrance of the reactor,

$$C_\mathrm{b}=C_0\quad \text{at } z=0. \tag{7}$$

Equation (6) can be integrated to give the concentration of the species at the bed exit C_out, and the corresponding conversion X can be calculated according to the definition

$$X=\frac{C_0-C_\mathrm{out}}{C_0}\times 100\%. \tag{8}$$

Subsequently, the parameters that characterize the mechanisms of adsorption and/or reaction on the surface under restrictive intraparticle diffusion were estimated by fitting the corresponding model into the experimental data using the least-squares method on MATLAB.

4. Results and discussion

4.1. Disappearance of metalloporphyrins on alumina

4.1.1. Mechanistic studies

The disappearance of VO-EP and Ni-EP on pure alumina was investigated under different temperatures (523–613 K) and volumes of extrudates (11 and 22 ml) at the same flow rate (16 ml/h). Although a clean model reaction system was employed, the results presented in Fig. 2 in the form of the apparent conversions of the metalloporphyrins vs time on stream still exhibited very complex patterns.

Under the conditions of these runs, thermal decomposition of the species was found to have a fixed contribution to the apparent conversions (3.5 wt% at most), which was not considered to be significant in interpreting the behavior of the metalloporphyrins on alumina. On the contrary, alumina that is a well-known adsorbent for separating porphyrinic species by “dry column” chromatography [46] was reported to have some transient capacity of demetallization [31]. A number of studies directly suggested that metalloporphyrins were adsorbed on the surface of alumina at room temperature or under hydroprocessing conditions [31,49,51–54]. Thus, the initially very high but gradually decreasing activity was attributed to the declining adsorption of the metalloporphyrins on alumina when the available sites were continuously occupied. Furthermore, when the adsorbed species were desorbed thermally in two runs (VP-4 and NiP-3 in Figs. 2a and 2b), the lost capacity of alumina

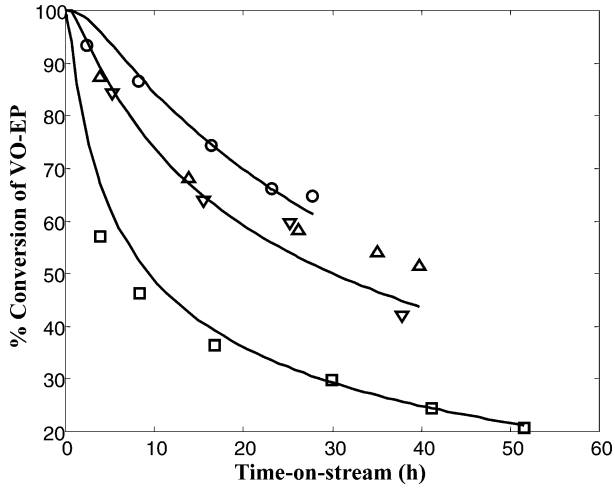

(a)

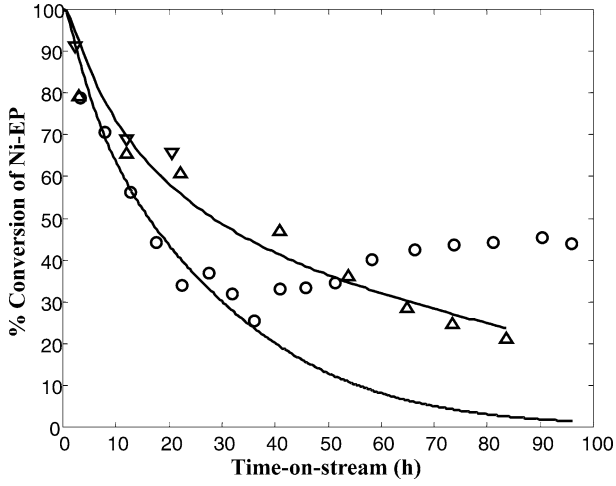

(b)

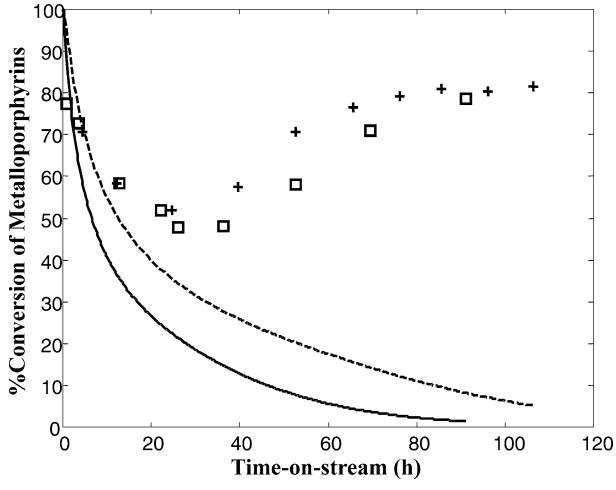

(c)

Fig. 2. Time course of the apparent conversions of metal etioporphyrins on alumna: (a) vanadyl etioporphyrin (VO-EP) in the runs VP-3 (□), VP-4 (▽), VP-4 (△) that was repeated after being heated at 673 K for about 24 h without feeding, and VP-6 (○); (b) nickel etioporphyrin (Ni-EP) in the runs NiP-3 (△), NiP-3 (▽) that was repeated after being heated at 673 K for about 24 h without feeding, and NiP-5 (○); (c) VO-EP and Ni-EP in the runs VP-5 (+) and NiP-4 (□). Solid and dashed lines represent the modeling results with the adsorption mechanism (dashed line represents VO-EP).

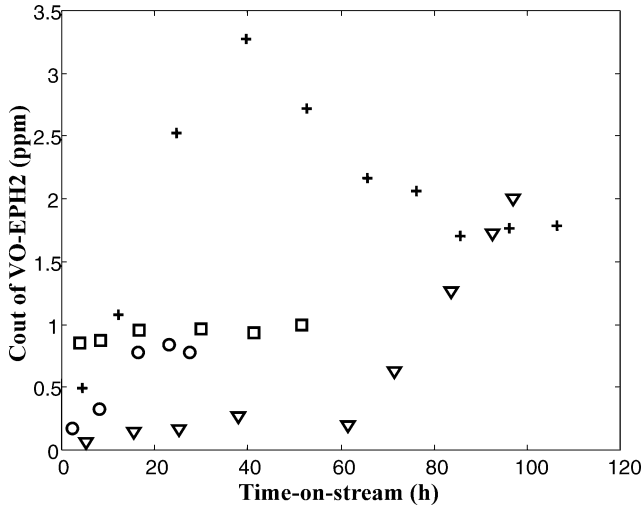

(a)

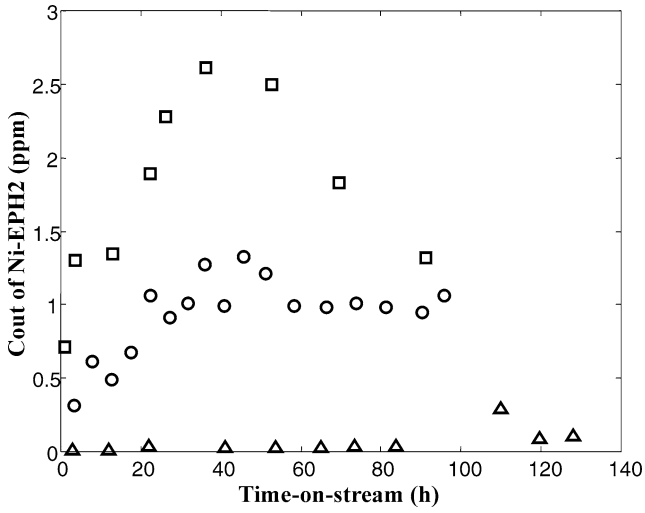

(b)

Fig. 3. Time course of the outlet concentrations of the dihydrogenated species with alumina: (a) vanadyl etiochlorin (VO-EPH$_2$) in the runs VP-3 (□), VP-4 (▽), VP-5 (+), and VP-6 (○); (b) nickel etiochlorin (Ni-EPH$_2$) in the runs NiP-3 (△), NiP-4 (□), and NiP-5 (○).

was renewed completely, indicating that the adsorption was reversible.

Unexpectedly, three runs (VP-5, NiP-4, and NiP-5) showed a rising activity in the latter parts instead of decaying to the end (Fig. 2). Moreover, the outlet concentrations of the dihydrogenated intermediates (VO-EPH$_2$ and Ni-EPH$_2$) were significantly higher in the latter periods than in the beginning for the three runs as shown in Fig. 3. Since catalytic cleavage of the metalloporphyrins under hydrogen was through a sequential mechanism via the hydrogenated intermediates [23–25], the autocatalytic effects proposed in several papers [38–41] were verified evidently. Notably, in the same figures (Fig. 3) the runs at a lower temperature (523 K, VP-3, VP-4, and NiP-3) did not exhibit the rising tendency before thermal desorption, confirming that the metalloporphyrins were dominantly adsorbed on the surface without being dissociated. Once the species were deconstructed to

Table 3
Modeling the disappearance of metalloporphyrins on alumina

Mechanism	Parameter		Feed	
			VO-EP	Ni-EP
Adsorption	ΔH (kJ/mol)		-7.86 ± 1.08	-30.41 ± 6.03
	K_{T_0} (10^{-3} m^3/g metal)		26.02 ± 0.68	9.67 ± 1.18
	ΔE_D (kJ/mol)		21.07 ± 1.50	15.01 ± 14.38
	D_{T_0} (10^{-6} cm^2/s)		2.56 ± 0.18	2.74 ± 0.51
	Calculated adsorption	523 K	30.46 ± 1.03	17.81 ± 3.06
	Equilibrium constant K	593 K	24.61 ± 0.67	7.80 ± 1.01
	(10^{-3} m^3/g metal)	613 K	23.36 ± 0.70	6.38 ± 0.94
	Calculated effective	523 K	1.67 ± 0.13	2.02 ± 0.69
	Diffusivity D_e	593 K	2.97 ± 0.21	3.04 ± 0.64
	(10^{-6} cm^2/s)	613 K	3.41 ± 0.25	3.36 ± 0.91
Autocatalytic reaction	Largest K_{appA} obtained (10^{-10} m$^{2.5}$ g-metal$^{-0.5}$ MPa$^{-0.7}$ h^{-1})	593 K	9.71 (VP-5)	9.99 (NiP-4)

ΔH, adsorption enthalpy; K_{T_0}, adsorption equilibrium constant at reference temperature (573 K); ΔE_D, activation energy of the effective diffusivity; D_{T_0}, effective diffusivity at reference temperature (573 K); K_{appA}, apparent rate constant of the autocatalytic reaction deriving from the metal deposition.

leave some metal deposits on alumina as in VP-4 and NiP-3, the catalytic effects were shown immediately in the forms of the rising outlet concentrations of the intermediates (Fig. 3) and the slightly higher conversions than before (Fig. 2).

4.1.2. Model building

Subsequently, the adsorption mechanism was tried to model the declining part of the metalloporphyrin disappearance on alumina, neglecting the influences of the thermal and the autocatalytic reactions. Specifically, in each run the adsorption mechanism was applicable from the beginning to the lowest point of the conversions, avoiding the part of the rising activity (Fig. 2).

Metalloporphyrins have been found mostly lying flat on the catalyst surface with which the plane of the molecule parallels in many papers [53,55–57]. In the modeling, a molecule of etio-type metalloporphyrins was assumed to occupy a 1.5 × 1.5-nm square [23,58]. Then the saturation capacity per unit surface area q_0^* was calculated to be 3.76×10^{-5} g V/m^2 for VO-EP and 4.33×10^{-5} g Ni/m^2 for Ni-EP. In addition, the temperature dependence of the adsorption equilibrium constant K was described by the van't Hoff equation, which was formulated as

$$K = K_{T_0} \exp\left(-\frac{\Delta H}{RT} + \frac{\Delta H}{RT_0}\right), \tag{9}$$

$$K_{T_0} = K_0 \exp\left(-\frac{\Delta H}{RT_0}\right), \tag{10}$$

where K_{T_0} denotes the adsorption equilibrium constant at the reference temperature, R is the gas constant (8.314 J mol^{-1} K^{-1}), ΔH represents the adsorption enthalpy that has a negative thermodynamic value, T_0 is the reference temperature that is usually the middle temperature (573 K in this study), and K_0 is the preexponential factor. The temperature dependence of the effective diffusivity D_e was expressed by an equation analogous to the Arrhenius equation [59], which was given as

$$D_e = D_{T_0} \exp\left(-\frac{\Delta E_D}{RT} + \frac{\Delta E_D}{RT_0}\right), \tag{11}$$

$$D_{T_0} = D_{e_0} \exp\left(-\frac{\Delta E_D}{RT_0}\right), \tag{12}$$

where D_{T_0} denotes the effective diffusivity at the reference temperature, ΔE_D represents the activation energy of the effective diffusivity, and D_{e_0} is the preexponential factor. So in each case four parameters needed estimating empirically, which were obtained by fitting the adsorption model into all the experimental sets of VO-EP or Ni-EP in the applicable range.

As given in Table 3, the calculated D_e was in the order of 10^{-6} cm^2/s for both of the metalloporphyrins under all the experimental temperatures, which agreed well with the published results [54,58,60]. The activation energies of D_e, which were 21.07 ± 1.50 kJ/mol for VO-EP and 15.01 ± 14.38 kJ/mol for Ni-EP, were weakly dependent upon temperature as expected. Besides, the adsorption enthalpy was -7.86 ± 1.08 kJ/mol for VO-EP and -30.41 ± 6.03 kJ/mol for Ni-EP, suggesting a very weak association of the metalloporphyrins with alumina [23]. The adsorption model predictions on the apparent conversions are presented in solid and dashed lines in Fig. 2. For the runs VP-5, NiP-4, and NiP-5, the calculated lines were extended to the end to illustrate the theoretical development of the conversions due purely to adsorption. It was not surprising that the predictions fit the experimental data reasonably well except in runs VP-5 and NiP-4, implying that the adsorption mechanism is a dominating factor for these runs in the calculation range.

Unfortunately, the results in runs VP-5 and NiP-4 deviated from the adsorption model predictions very seriously even in the calculation period (from the beginning to the lowest conversion). Since the two runs were not performed at the

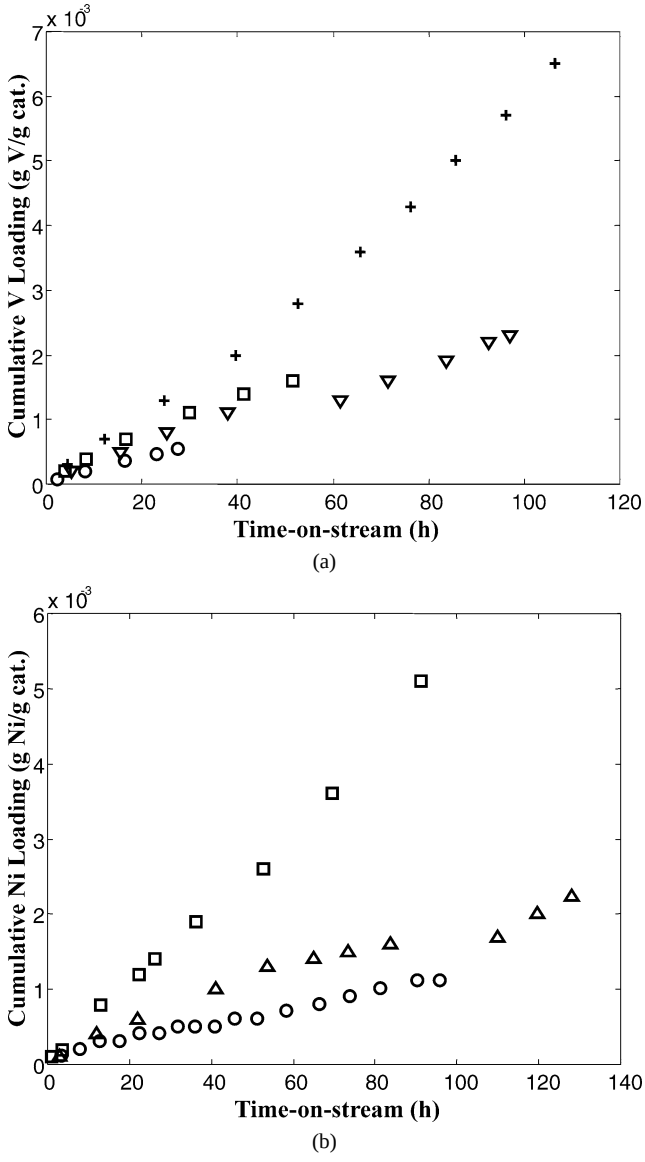

Fig. 4. Time course of the cumulative metal loading on alumina: (a) vanadium in the runs VP-3 (□), VP-4 (▽), VP-5 (+) and VP-6 (○); (b) nickel in the runs NiP-3 (△), NiP-4 (□), NiP-5 (○).

highest temperature, thermal degradation of the metalloporphyrins could not result in the highly added activity beyond the adsorption. Fig. 4 shows the actual cumulative loading of the metals on alumina, which was estimated using a polynomial curve-fitting method. Apparently, the metal loading was significantly higher in runs VP-5 and NiP-4 than in the others with the same running length, which resulted from the least particle volume and the highest feed concentration of the two runs. Correspondingly, the outlet concentrations of the dihydrogenated intermediates were higher with the time on stream in the two runs than in the others as well (Fig. 3). Thereby, it was concluded that the autocatalytic reactions deriving from the metal deposition contributed to the apparent conversions in runs VP-5 and NiP-4 and even greater than in the runs at a higher temperature (613 K, runs VP-6 and NiP-5).

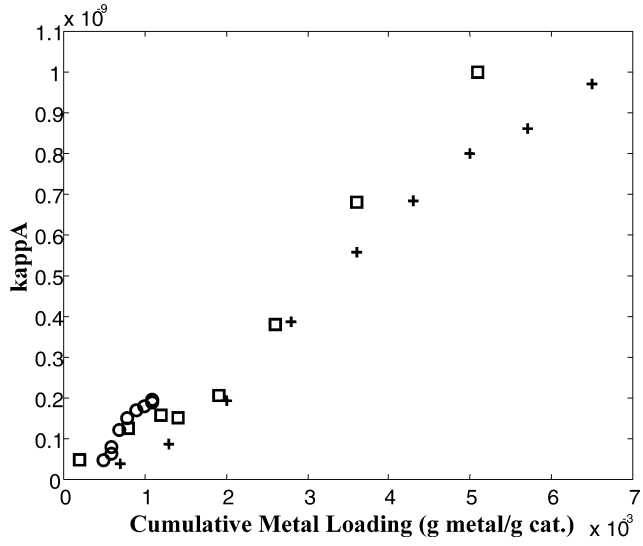

Fig. 5. Apparent rate constants of the autocatalytic reactions k_{appA} versus cumulative metal loading on alumna in the runs VP-5, NiP-4, and NiP-5. Symbols: (+) VP-5; (□) NiP-4; (○) NiP-5. Conditions: 7 MPa.

Based on the discussion above, the added activity is not explained by the adsorption mechanism in the whole time on stream of in runs VP-5, NiP-4, and NiP-5. Instead the added activity was ascribed to a growing catalytic activity deriving from the metal accumulation on the surface. It will be shown in the next section that the apparent disappearance rate due to the catalytic reaction was 1.5 order of magnitude dependent on the metal concentration ($n = 1.5$) and 0.7 order of magnitude dependent on the total pressure ($m = 0.7$). Thus, the apparent rate constants of the autocatalytic reactions k_{appA} that should be a function of the temperature and the metal accumulation were calculated by

$$k_{\text{appA}} = \frac{\text{LHSV}}{\rho_{\text{b}}} \frac{1}{P^m} \frac{1}{C_0^{n-1}} \frac{1-(1-X_A)^{1-n}}{1-n}, \tag{13}$$

in which X_A represents the added conversion that was not explained by the adsorption mechanism, ρ_{b} is the density of the bed, and LHSV denotes the liquid hourly space velocity. The results are presented in Fig. 5 by plotting k_{appA} against the cumulative metal loading on the particles. A linear increase of the rate constants with the cumulative metal loading verified the above analysis.

Thereby, the complicated disappearing patterns of the metalloporphyrins on alumina were mainly assigned to the combined effects of a declining adsorption on alumina and a growing catalytic reaction deriving from the metal deposition.

4.2. Disappearance of metalloporphyrins on HDM catalysts

4.2.1. Adsorption or steady-state reaction

The adsorption of Ni-EP on the HDM catalyst TK-710 was studied at 523 K in run NiP-6. During the experiment, nitrogen was introduced to prevent the catalytic reaction,

Table 4
Modeling the disappearance of metalloporphyrins on HDM catalysts

Mechanism	Parameter	Feed	
		VO-EP	Ni-EP
Adsorption	K (10^{-3} m^3/g metal)	300[a]	31.28 ± 18.67[b]
	D_e (10^{-7} cm^2/s)		1.49 ± 1.23[b]
Steady-state catalytic reaction	m	0.7	0.7
	n	1.5	1.5
	E_{app} (kJ/mol)	59.83 ± 5.18	66.52 ± 13.48
Simultaneous adsorption and reaction with N-containing poison (573 K, VP-7)	K (10^{-3} m^3/g metal)	350 ± 2.6	
	D_e (10^{-7} cm^2/s)	6.62 ± 1.19	
	k_i (10^{-9} $m^{2.5}$ g-V$^{-0.5}$ $MPa^{-0.7}$ h^{-1})	3.21 ± 0.40	
	K_{appC} (10^{-9} $m^{2.5}$ g-V$^{-0.5}$ $MPa^{-0.7}$ h^{-1})	2.04	
	K_{appC} (10^{-9} $m^{2.5}$ g-V$^{-0.5}$ $MPa^{-0.7}$ h^{-1})	3.11(593 K)	

K, adsorption equilibrium constant for the Langmuir isotherm; D_e, effective diffusivity; m, reaction order with respect to the total pressure; n, surface reaction order; E_{app}, apparent activation energy of the catalytic reaction; k_i, rate constant of the intrinsic surface reaction; k_{appC}, apparent rate constant of the catalytic reaction deriving from the catalyst.

[a] 543 K, estimated from the data in Ref. [49].

[b] 523 K, NiP-6.

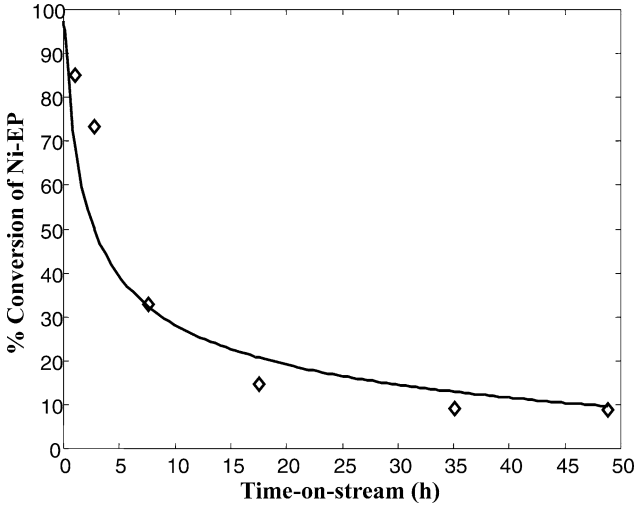

Fig. 6. Time course of the apparent conversions of nickel etioporphyrin (Ni-EP) on the HDM catalyst under N_2 in the run NiP-6. Solid line represents the modeling results with the adsorption mechanism. Conditions: 523 K, 5 MPa.

which was realized through the observation that the dihydrogenated intermediate was not detected at the bed exit. Then the adsorption model was applied to the time course of the disappearances, and the results are shown in Fig. 6 and Table 4. The adsorption equilibrium constant of VO-EP at 543 K on TK-710 was roughly estimated to be 0.3 m^3/g-V from the transient period data in a previous work [49], in which an extremely quick drop of the concentration was blamed on the VO-EP adsorption on the catalyst. It was not surprising that a larger equilibrium constant and a smaller effective diffusivity were obtained on the HDM catalyst than on alumina. The active metals loaded on the support were supposed to attract more reactants. Besides, these magnitudes of the equilibrium constants have been found in studies using metal tetraphenylporphyrins and metal tetra(3-methylphenyl)porphyrins [61]. Since a stronger adsorption resulted in a greater drag force, the smaller effective diffusivity was attributed to the restrictive effect [25].

The steady catalytic HDM reactions of the metalloporphyrins were investigated in runs VP-8 and NiP-7 at different temperatures (503–593 K), total pressures (2–8 MPa), and flow rates (17.5–46 ml/h), and the results are also presented in Table 4. The disappearance rate due to the catalytic reaction was found to be 1.5 order of magnitude with respect to the metal concentration and 0.7 order of magnitude with respect to the total pressure. The apparent activation energies of the catalytic reactions calculated were 59.83 ± 5.18 kJ/mol for VO-EP and 66.52 ± 13.48 kJ/mol for Ni-EP, which were in the range of a typical hydrogenation reaction and are in good agreement with the studies of Morales et al. [62].

4.2.2. Simultaneous adsorption and reaction

The time-course conversions of VO-EP on the HDM catalyst TK-710 were studied at 573 K under hydrogen in the run VP-7, in which 0.05% N in 2,6-dimethylpyridine presented in the stream. A typical transient period of the activity is exhibited in Fig. 7, which was characterized by high activity in the beginning and soon decayed to a quasi-equilibrium state. This period was thought to correspond to the initially decaying stage of the HDM catalysts under industrial conditions.

Several researchers have reported the transient period in their experiments with metalloporphyrins [46,49,51], but few have made an effort to understand it. Bonné et al. described the initial period as a phenomenon of catalyst deactivation; however, they concluded that the metals did not deposit on the active sites [63]. Since catalyst deactivation is usually referred to an activity loss of some active sites, the decreasing activity could not be interpreted as deactivation if the active phase were not involved or altered. As a matter of fact, the conclusion could be drawn from their study that the decay of the activity was in association with

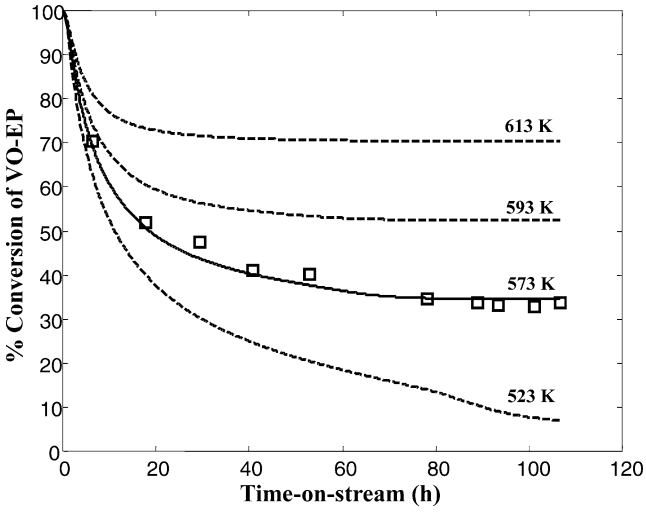

Fig. 7. Time course of the apparent conversions of vanadyl etioporphyrin (VO-EP) with the HDM catalyst in the run VP-7. Solid line represents the modeling results with the simultaneous adsorption and reaction mechanism. Dashed lines represent the simulation results when the experiments were run at different reaction temperatures. Conditions: 573 K, 5 MPa.

the alumina support, which was in agreement with our results that the metalloporphyrins were adsorbed on alumina. Therefore, a new mechanism, the simultaneous adsorption and reaction mechanism, was proposed for the initial period in this work: the apparent activity stemmed from a nearly constant catalytic activity of the active phase coupled with an extra adsorption on the alumina support.

In summary, the model based on the new mechanism including neither thermal reactions nor autocatalytic reactions fit the experimental data very well as shown in Fig. 7 in the solid line, while the calculated values of the characteristic parameters K, D_e, and k_i were given in Table 4. As expected, a larger equilibrium constant and a smaller effective diffusivity were also obtained for VO-EP on the HDM catalyst than on alumina. The corresponding apparent rate constant due to the catalytic reaction k_{appC} at 573 K was calculated as well. Since the apparent activation energy for VO-EP has been determined, the value of k_{appC} at 593 K was estimated as shown in Table 4.

In Fig. 2c, the apparent conversions fell off near the end of VP-5, indicating that further accumulation of the metals would not increase the autocatalytic reaction very much. The largest value of the apparent rate constant due to the autocatalytic reaction k_{appA} at 593 K (Table 3) was only a third of k_{appC} of the commercial HDM catalyst even with N-containing poison (Table 4). To make the matter worse, vanadium catalysts supported by alumina were found to have much lower hydrogenolysis activity than molybdenum-based hydroprocessing catalysts while the hydrogenation activity was comparable [64]. Therefore, it was concluded that the metal deposits were far inferior to commercial HDM catalysts in removing the metals from the stream. Consequently, the poisoning deactivation mechanism was ruled out in explaining the initial decay of the HDM catalysts, since the autocatalytic reaction was incapable of making up the activity loss in the steady stage.

It was worthy of note that the limited sites of the catalysts for the adsorption were continuously occupied with the time on stream, so different experimental methods and conditions could disguise the added activity. The probable cases were stabilizing the catalysts in the first place [46,49,51], loading the catalysts with metal deposits prior to the experiments [34,35,37,41], using an extremely high LHSV or a very large ratio of feed to catalyst [48,50], and employing a very high feed concentration accompanying the crushed catalysts [36,47]. With respect to the catalyst properties, the most important factor was the relatively active strength between the adsorption and the reaction. It was well known that both adsorption and reactions were temperature dependent but responded to temperature changes in opposite directions. The dashed lines in Fig. 7 are the results that simulate the influence of different reaction temperatures on the apparent conversions using the simultaneous adsorption and reaction mechanism. Obviously, the initial period was reduced with the increase of the reaction temperatures.

In reality, a lower intrinsic activity and a larger capacity for deposit-storage distinguished the HDM catalysts from other hydroprocessing catalysts. The process with smaller LHSV was always started at a reaction temperature as low as possible. Therefore, the industrial practice fully utilized the adsorption capacity of the alumina carriers, which was believed not to be negligible to the initial apparent conversions.

5. Conclusions

Three factors are generally responsible for the apparent conversions of the metalloporphyrins in a fixed-bed reactor: thermal decomposition, adsorption on the alumina support, and catalytic reactions. The thermal degradation that has a fixed contribution to the apparent conversions is negligible when the reaction temperature is below 613 K. The adsorption of the metalloporphyrins on alumina is quantitatively confirmed in this work, and the metal deposits are proven to have some catalytic activity especially hydrogenation activity instead of being a poison. The autocatalytic activity is increased with the metal accumulation on the surface to some extent, but is still far inferior to the commercial HDM catalysts due to lack of some active elements such as molybdenum. Therefore, the poisoning deactivation is not convincing as an explanation of the initially decaying period of the HDM catalysts, since the autocatalytic effects are not able to compensate the activity loss in the steady stage. Instead, for the first time a simultaneous adsorption and reaction mechanism is proposed for the initial declining activity of the HDM catalysts in this study. The initial apparent activity is interpreted as an effect of a nearly constant catalytic activity of the active phase in combination with a decreasing adsorption on the alumina support when the available sites are gradu-

ally and continuously occupied. As a result, the new model fits the experimental data reasonably well. In practice, the HDM unit loaded with low intrinsic-activity catalysts is always started at a reaction temperature as low as possible, so the process is just run under conditions to fully utilize the adsorption capacity that is not negligible to the initial apparent conversions.

Acknowledgment

The authors are grateful for economic financing of the experiments from the Swedish National Board of Energy.

Appendix A. Nomenclature

A_c	Cross-sectional area of the bed
C_b	Concentration of the species in the bulk stream
C_i	Concentration of the species inside the particle
C_0	Concentration of the species in the feed
C_{out}	Concentration of the species at the bed exit
D_e	Effective diffusivity
D_{e_0}	Preexponential factor
D_{T_0}	Effective diffusivity at the reference temperature
E_{app}	Apparent activation energy of the catalytic reaction
ΔE_D	Activation energy of the effective diffusivity
ΔH	Adsorption enthalpy
K	Adsorption equilibrium constant for the Langmuir isotherm
K_{T_0}	Adsorption equilibrium constant at the reference temperature
K_0	Preexponential factor
k_{appA}	Apparent rate constant of the autocatalytic reaction deriving from the metal deposition
k_{appC}	Apparent rate constant of the catalytic reaction deriving from the catalyst
k_i	Rate constant of the intrinsic surface reaction
LHSV	Liquid hourly space velocity
m	Reaction order with respect to the total pressure
n	Surface reaction order
N_i	Disappearance rate of the specie per unit volume of the particle
P	Total pressure
q	Adsorbed quantity of the specie on the surface per unit weight
q^*	Adsorbed quantity of the specie on the surface per unit surface area
q_0^*	Maximum adsorbed quantity of the specie on the surface per unit surface area
R	Gas constant ($8.314\,\mathrm{J\,mol^{-1}\,K^{-1}}$)
R_0	Particle radius
r	Radial position inside the particle
S_a	Surface area per unit mass of the particle
T	Reaction temperature
T_0	Reference temperature
t	Process time
v_0	Volumetric flow rate
X	Conversion
X_A	Added conversion that is not explained by the adsorption mechanism
z	Axial position of the catalyst bed
ε	Bed void fraction
ρ_b	Density of the catalyst bed
ρ_c	Density of the catalyst particle

References

[1] E. Newson, Ind. Eng. Chem. Process Des. Dev. 14 (1975) 27.
[2] F.M. Dautzenberg, J. van Klinken, K.M.A. Pronk, S.T. Sie, J.B. Wijffels, ACS Symp. Ser. 65 (1978) 254.
[3] A. Nielsen, B.H. Cooper, A.C. Jacobsen, Prepr. Am. Chem. Soc., Div. Pet. Chem. 26 (1981) 440.
[4] P.W. Tamm, H.F. Harnsberger, A.G. Bridge, Ind. Eng. Chem. Process Des. Dev. 20 (1981) 262.
[5] P.N. Hannerup, A.C. Jacobsen, Prepr. Am. Chem. Soc., Div. Pet. Chem. 28 (1983) 576.
[6] H. Koyama, E. Nagai, H. Kumagai, ACS Symp. Ser. 634 (1996) 208.
[7] T. Ohtsuka, Catal. Rev. Sci. Eng. 16 (1977) 291.
[8] E. Furimsky, Ind. Eng. Chem. Prod. Res. Dev. 17 (1978) 329.
[9] M. Ternan, E. Furimsky, B.I. Parson, Fuel Process. Technol. 2 (1979) 45.
[10] R. Galiasso, R. Blanco, C. Gonzalez, N. Quinteros, Fuel 62 (1983) 817.
[11] D.S. Thakur, M.G. Thomas, Ind. Eng. Chem. Process Des. Dev. 23 (1984) 349.
[12] D.S. Thakur, M.G. Thomas, Appl. Catal. 15 (1985) 197.
[13] M. Shimura, Y. Shiroto, C. Kakeuchi, Ind. Eng. Chem. Fundam. 25 (1986) 330.
[14] A. Nishijima, H. Shimada, Y. Yoshimura, T. Sato, N. Matsubayashi, Stud. Surf. Sci. Catal. 34 (1987) 39.
[15] F. Diez, B.C. Gates, J.T. Miller, D.J. Sajkowski, S.G. Kukes, Ind. Eng. Chem. Res. 29 (1990) 1999.
[16] M. Absi-Halabi, A. Stanislaus, D.L. Trimm, Appl. Catal. 72 (1991) 193.
[17] J. Bartholdy, B.H. Cooper, Prepr. Am. Chem. Soc., Div. Pet. Chem. 38 (1993) 386.
[18] D.L. Trimm, in: M. Absi-Halabi, et al. (Eds.), Catalysts in Petroleum Refining and Petrochemical Industries, Elsevier, Amsterdam, 1995, p. 65.
[19] S.M. Richardson, H. Nagaishi, M.R. Gray, Ind. Eng. Chem. Res. 35 (1996) 3940.
[20] M. Marafi, A. Stanislaus, Appl. Catal. 159 (1997) 259.
[21] M.R. Gray, Y. Zhao, C.M. McKnight, D.A. Komar, J.D. Carruthers, Energy Fuels 13 (1999) 1037.
[22] H. Seki, M. Yoshimoto, Sekiyu Gakkaishi 44 (2001) 259.
[23] R.J. Quann, R.A. Ware, C.H. Hung, J. Wei, Adv. Chem. Eng. 14 (1988) 95.
[24] H. Topsoe, B.S. Clausen, F.E. Massoth, in: J.R. Anderson, M. Boudart (Eds.), Hydrotreating Catalysis: Science and Technology, in: Catalysis—Science and Technology, vol. 11, Springer, Berlin, 1996.
[25] E. Furimsky, F.E. Massoth, Catal. Today 52 (1999) 381.
[26] P.N. Hannerup, A.C. Jacobsen, Prepr. Am. Chem. Soc., Div. Pet. Chem. 28 (1981) 262.
[27] B.J. Ahn, J.M. Smith, AIChE J. 30 (1984) 739.
[28] B.J. Johnson, F.E. Massoth, J. Bartholdy, AIChE J. 32 (1986) 1980.
[29] G. Gualda, S. Kasztelan, Stud. Surf. Sci. Catal. 88 (1994) 145.
[30] J. Bartholdy, B.H. Cooper, in: M. Absi-Halabi, et al. (Eds.), Catalysts in Petroleum Refining and Petrochemical Industries, Elsevier, Amsterdam, 1995, p. 117.

[31] G. Gualda, S. Kasztelan, J. Catal. 161 (1996) 319.
[32] C.H. Bartholomew, Chem. Eng. 12 (1984) 96.
[33] T.H. Fleisch, B.L. Meyers, J.B. Hall, G.L. Ott, J. Catal. 86 (1984) 147.
[34] J. van Doorn, J.A. Moulijn, Catal. Today 7 (1990) 257.
[35] E.P.H. Rautiainen, J. Wei, Chem. Eng. Commun. 98 (1990) 113.
[36] B.J. Smith, J. Wei, J. Catal. 132 (1991) 1.
[37] C.-S. Kim, F.E. Massoth, Fuel Process. Technol. 35 (1993) 289.
[38] H. Toulhoat, J.C. Plumail, G. Martino, Y. Jacquin, Prepr. Am. Chem. Soc., Div. Pet. Chem. 30 (1985) 85.
[39] C. Takeuchi, S. Asaoka, S. Nakata, Y. Shiroto, Prepr. Am. Chem. Soc., Div. Pet. Chem. 30 (1985) 96.
[40] J. Devanneaux, J.P. Gallez, L. Mariette, P.A. Engelhard, Prepr. Am. Chem. Soc., Div. Pet. Chem. 30 (1987) 84.
[41] S. Dejonghe, R. Hubaut, J. Grimblot, J.P. Bonnelle, T. des Courieres, Catal. Today 7 (1990) 569.
[42] J.P. Janssen, G. Elst, E.G. Schrikkema, A.D. van Langeveld, S.T. Sie, J.A. Moulijn, Recl. Trav. Chim. Pays-Bas 115 (1996) 465.
[43] E.W. Baker, S.E. Palmer, in: D. Dolphin (Ed.), The Porphyrins, Vol. I, Academic Press, New York, 1978, Chap. 11.
[44] E. Baker, D. Elliott, ACS Symp. Ser. 376 (1987) 228.
[45] P. Abrahamsson, Licentiate thesis, Chalmers University of Technology, Göteborg, 1991.
[46] R. Agrawal, J. Wei, Ind. Eng. Chem. Process Des. Dev. 23 (1984) 505.
[47] R.A. Ware, J. Wei, J. Catal. 93 (1985) 100.
[48] R.L.C. Bonné, P. van Steenderen, A.D. van Langeveld, J.A. Moulijn, Ind. Eng. Chem. Res. 34 (1995) 3801.
[49] F.X. Long, B.S. Gevert, J. Catal. 200 (2001) 91.
[50] R.L.C. Bonné, P. van Steenderen, J.A. Moulijn, Appl. Catal. A 206 (2001) 171.
[51] C.W. Hung, J. Wei, Ind. Eng. Chem. Process Des. Dev. 19 (1980) 257.
[52] A. Morales, R. Galiasso, Fuel 61 (1982) 13.
[53] A. Morales, C. Marrero, R. Galiasso, in: Proceedings, 8th International Congress on Catalysis, Berlin, 1984, Vol. II, Dechema, Frankfurt am Main, 1984, p. 329.
[54] R. Galiasso, A. Morales, Appl. Catal. 7 (1997) 57.
[55] P.C.H. Mitchell, Catal. Today 7 (1990) 439.
[56] P.C.H. Mitchell, C.E. Scott, Catal. Today 7 (1990) 467.
[57] M. Loos, A. Ascone, P. Friant, M.F. Ruiz-Lopez, J. Goulon, J.M. Barbe, N. Seglet, R. Guilard, D. Faure, T. des Courieres, Catal. Today 7 (1990) 497.
[58] R. Agrawal, J. Wei, Ind. Eng. Chem. Process Des. Dev. 23 (1984) 515.
[59] W.J. Thomas, B. Crittenden, Adsorption Technology and Design, Butterworth-Heinemann, Boston, 1998.
[60] S.Y. Lee, J.D. Seader, C.H. Tsai, F.E. Massoth, Ind. Eng. Chem. Res. 30 (1991) 29.
[61] H.J. Chen, F.E. Massoth, Ind. Eng. Chem. Res. 27 (1988) 1629.
[62] A. Morales, J.J. Garcia, R. Prada, O. Abrams, L. Katan, in: Proceedings, 8th International Congress on Catalysis, Berlin, 1984, Vol. II, Dechema, Frankfurt am Main, 1984, p. 341.
[63] R.L.C. Bonné, P. van Steenderen, A.E. van Diepen, J.A. Moulijn, Appl. Catal. A 108 (1994) 171.
[64] R.L.C. Bonné, P. van Steenderen, J.A. Moulijn, Bull. Soc. Chim. Belg. 100 (1991) 877.